Journal of Translational Medicine

RESEARCH

Open Access

A novel model for predicting postoperative liver metastasis in R0 resected pancreatic neuroendocrine tumors: integrating computational pathology and deep learning-radiomics

Mengke Ma[1,2,3†], Wenchao Gu[4,5,6†], Yun Liang[2,7], Xueping Han[1,2,3], Meng Zhang[1,2,3], Midie Xu[1,2,3], Heli Gao[2,7,8*], Wei Tang[2,5*] and Dan Huang[1,2,3*]

Abstract

Background Postoperative liver metastasis significantly impacts the prognosis of pancreatic neuroendocrine tumor (panNET) patients after R0 resection. Combining computational pathology and deep learning radiomics can enhance the detection of postoperative liver metastasis in panNET patients.

Methods Clinical data, pathology slides, and radiographic images were collected from 163 panNET patients post-R0 resection at Fudan University Shanghai Cancer Center (FUSCC) and FUSCC Pathology Consultation Center. Digital image analysis and deep learning identified liver metastasis-related features in Ki67-stained whole slide images (WSIs) and enhanced CT scans to create a nomogram. The model's performance was validated in both internal and external test cohorts.

Results Multivariate logistic regression identified nerve infiltration as an independent risk factor for liver metastasis ($p < 0.05$). The Pathomics score, which was based on a hotspot and the heterogeneous distribution of Ki67 staining, showed improved predictive accuracy for liver metastasis (AUC = 0.799). The deep learning-radiomics (DLR) score achieved an AUC of 0.875. The integrated nomogram, which combines clinical, pathological, and imaging features, demonstrated outstanding performance, with an AUC of 0.985 in the training cohort and 0.961 in the validation

†Mengke Ma and Wenchao Gu have contributed equally to this work and share first authorship.

*Correspondence:
Heli Gao
gaoheli@fudanpci.org
Wei Tang
tangwei105@163.com
Dan Huang
danhuang@shca.org.cn

Full list of author information is available at the end of the article

cohort. High-risk group had a median recurrence-free survival of 28.5 months compared to 34.7 months for the low-risk group, showing significant correlation with prognosis ($p < 0.05$).

Conclusion A new predictive model that integrates computational pathologic scores and deep learning-radiomics can better predict postoperative liver metastasis in panNET patients, aiding clinicians in developing personalized treatments.

Keywords Pancreatic neuroendocrine tumors, Postoperative liver metastasis, Deep learning-radiomics, Computational pathology, Nomogram

Introduction

Pancreatic neuroendocrine tumors (panNETs) are rare, but their incidence has notably risen in recent years [1, 2]. These tumors have a strong tendency to spread to the liver, which significantly impacts patient survival [3–5]. Surgical resection, particularly complete resection (R0) of pancreatic lesions or resectable liver metastases, is commonly recommended for treating panNET patients, as it greatly improves the survival rate of patients with localized lesions [4, 6]. Postoperative liver metastasis is a crucial adverse prognostic factor for patients after surgical resection [7]. Currently, there is no consensus regarding the management and treatment strategies for patients with panNETs following R0 resection. Therefore, developing effective methods to predict postoperative liver metastasis is a top research priority and challenge.

Previous studies have shown that nomogram models based on textual data from clinical histories and pathological reports can predict postoperative recurrence and liver metastasis [8, 9]. Given the significant role of Ki67 proliferative activity in the diagnosis and prognosis of neuroendocrine neoplasms [10], we used a novel digital image analysis (DIA) algorithm to predict postoperative liver metastasis by analyzing Ki67-stained whole slide images (WSIs) [9]. This DIA algorithm can accurately and objectively calculate the Ki67 value in a region of interest (ROI), enabling manual counting with greater precision. More importantly, this DIA can analyze the spatial variability of Ki67 in panNETs, providing valuable insights into tumor heterogeneity. Computational pathology parameters, such as the Morisita-Horn (MH) index, were utilized to digitize the spatial distribution of Ki67-stained cells. These digital biomarkers can reflect the heterogeneity of proliferative activity and provide a novel perspective on observing the characteristics of panNETs from a heterogeneous standpoint based on ecological knowledge. Integrating the DIA Ki-67 index with the MH index enables a comprehensive assessment of panNETs that encompasses conventional Ki-67 quantification and tumor heterogeneity analysis. The use of composite computational pathology parameters may improve liver metastasis prediction in postoperative panNET patients.

Although CT is the standard method for detecting liver metastasis, it has limited accuracy in identifying microscopic metastasis. Recently, there has been growing interest in CT-based radiomics to improve the diagnosis and prognosis of patients with panNETs [8, 11]. In a previous study, we presented an innovative model that integrates radiomics and deep learning to predict lymph node metastasis in non-functional panNET patients [12]. This deep learning network was pretrained using radiomic data to create radiomic deep learning signatures. These signatures, extracted from contrast-enhanced CT images of primary pancreatic areas, can improve the prediction accuracy of tumor metastasis and patient outcomes for non-functional panNET patients. This finding suggested a correlation between CT imaging features and tumor metastasis. Consequently, further investigations are warranted to explore the relationships between these imaging characteristics and postoperative liver metastasis.

The novel Ki67 heterogeneity index and radiomics deep learning signature may offer deeper insight into tumor characteristics beyond clinicopathological information. This study is the first to analyze a combination of pathological, clinical, and CT features to develop a precise model for predicting liver metastases in postoperative panNET patients. This model may assist clinicians in developing appropriate management and treatment strategies for panNET patients after R0 resection.

Methods

Study patients

This retrospective study included panNET patients who underwent complete resection at Fudan University Shanghai Cancer Center (FUSCC) and the FUSCC Pathology Consultation Center between 2015 and 2022 (Fig. 1). The inclusion criteria were as follows: (a) confirmed neuroendocrine tumor through pathological examination, (b) primary lesion located in the pancreas, (c) achieved R0 resection for both the primary pancreatic lesion and synchronous liver metastasis if present, (d) postoperative liver condition confirmed by enhanced liver CT/MRI during follow-up, and (d) no other sites of metastasis. All patients from our hospital and non-affiliated hospitals were divided into two groups based on the occurrence of postoperative new-onset liver metastasis: the liver metastasis group and the non-liver metastasis group. Clinical information, including sex, age, site,

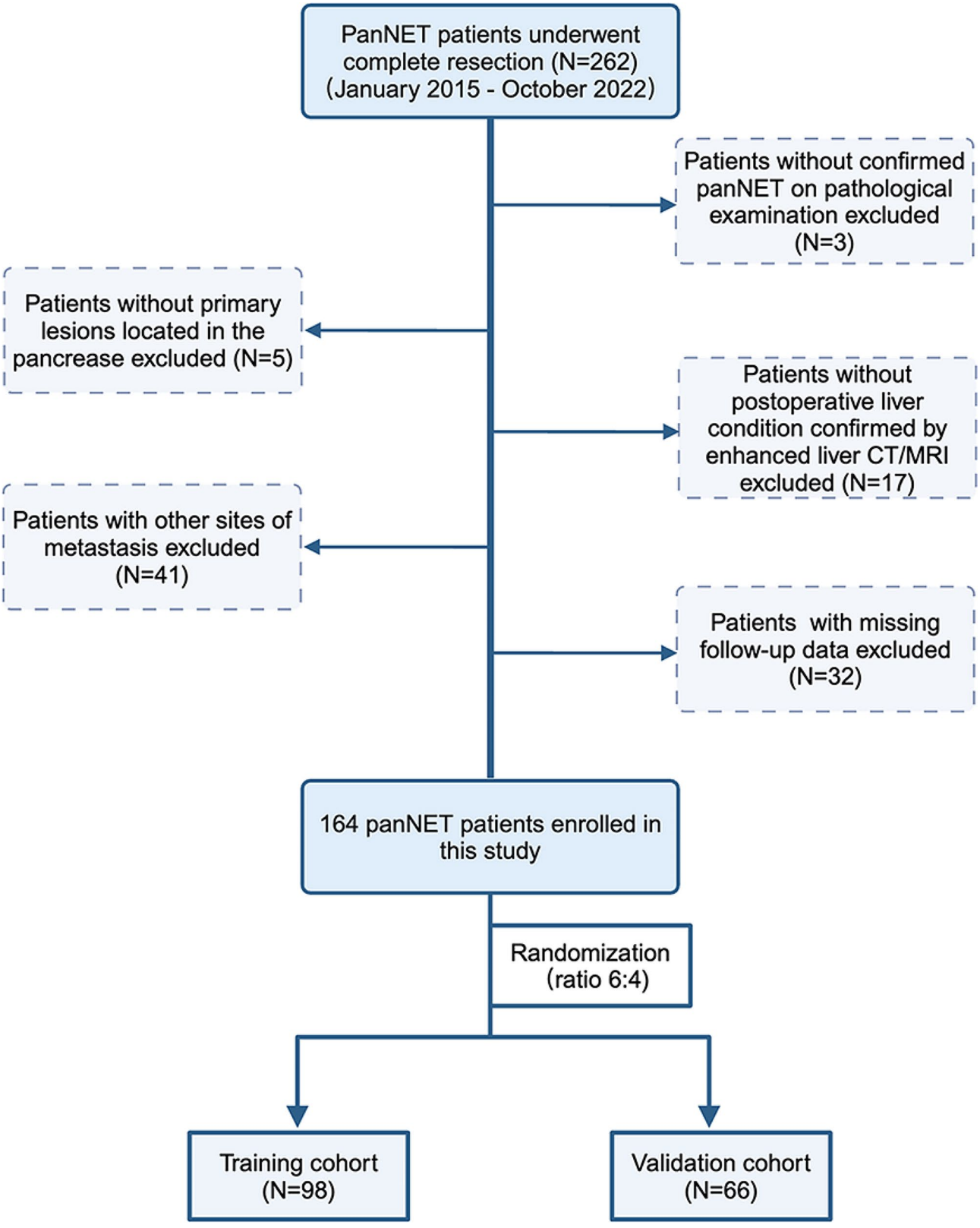

Fig. 1 Workflow of the patient selection process

tumor size, vascular invasion status, nerve infiltration status, tumor grade, T stage, and lymph node status, was collected from medical records. Pathological diagnoses were reviewed by pathologists (D.H. and M.Z.) and Ki67-stained slides were collected for each patient. Preoperative contrast-enhanced pancreatic/abdominal CT images were collected and reviewed by radiologists (Y.C. and W.T.). This retrospective study received approval from the ethical review committee of the World Health Organization of the Collaborating Center for Research in Human Production and the human ethics committee of FUSCC (No. 050432-4-2108).

Patient follow-up was conducted via either outpatient visits or telephone via the Tumor Registry at FUSCC. Recurrence and metastasis were detected through routine CT or MRI scans performed 6 months after surgery and subsequently annually from the initial follow-up. The follow-up period ended on January 11, 2024. Recurrence-free survival (RFS) was considered the interval from the date of surgery to the first occurrence/recurrence of liver metastasis or the last follow-up.

Computational pathology model

Ki67 staining was routinely performed using a Ki67 antibody (MIB-1 clone; Roche) on the Ventana automated Benchmark staining system (Ventana Medical Systems), following the manufacturer's instructions. The Ki67-stained slides were scanned to whole-slide images (WSIs) at 40× magnification with a resolution of 0.5 μm per pixel by the KF-pro-005 automatic digital slide scanning system (KFBIO Technology for Health). Our previous DIA enables the calculation of the Ki67 index in hotspot areas and the Morisita-Horn (MH) index in heterogeneous distributions. First, regions of interest (ROIs) were marked interactively by a pathologist (D.H.) and then divided into 500 to 1000 fields. Within these ROIs, hotspot candidate regions (HCRs) were identified based on a 1500-pixel grid. HCRs with more than 500 tumor cells were considered "valid HCRs". Second, a sliding window algorithm was utilized to identify positive cells and calculate the percentage of Ki67-positive cells in each valid HCR. To determine the Ki67 index, a pre-established model was applied to identify the highest positivity among all valid HCRs [9].

The algorithm of the MH index was used to quantitatively evaluate the spatial colocalization of the Ki67 parameters in the grid-based ROIs. The intra-field variability of the Ki67 score was calculated, and the MH index was calculated to reflect spatial heterogeneity across the WSIs, as described in our previous work [9].

$$MH = \frac{2\sum_i p_i^{neg} p_i^{pos}}{\sum_i (p_i^{neg})^2 + \sum_i (p_i^{pos})^2}$$

The value of the MH index ranges from 0 to 1, indicating that negative and positive nuclei are not similar or highly similar in spatial distribution.

Both the Ki67 index and MH index were recorded as pathomics signatures for each panNET patient. These signatures were then used in logistic regression to assign a "Pathomics score" for each patient.

Radiomics and deep learning model

The atrial phase of CT images was utilized for tumor segmentation using ITK-SNAP (version 4.0.2; http://www.itsnap.org). The methodology was consistent with our prior study [12]. Radiomic features were extracted using the Pyradiomics package in Python (version 3.7; https://github.com/Radiomics/pyradiomics). The deep learning features were derived from the maximum of the ROI slide using a convolutional neural network (ResNET101). Feature selection was conducted in three stages: (1) initially, images from 30 randomly selected patients were chosen for intraclass correlation coefficient (ICC) analysis. Features with an ICC value less than 0.8 were excluded; (2) then, patients were randomly divided into training and test cohorts at a ratio of 6:4. Based on the training cohort, the Mann–Whitney U test and Pearson correlation test were then applied to evaluate significant differences between the two groups and correlations with each feature. Features with an adjusted p value less than 0.05 according to the Mann–Whitney U test and a correlation coefficient smaller than 0.5 were retained and normalized using z-score. LASSO logistic regression was subsequently utilized to further decrease the number of features via 10-fold cross-validation. The machine learning method was conducted through the ridge algorithm, which led to the generation of both radiomics and deep learning scores. Ultimately, the deep learning-radiomics (DLR) score was derived using logistic regression to combine the radiomics and deep learning scores.

Construction of an integrated nomogram model

A novel nomogram model was developed to predict liver metastasis in panNET patients. This model combines the clinically independent risk factor and the Pathomics score from DIA with the DLR score from radiology, as illustrated in Fig. 2. The training and validation cohorts were selected as a random 6:4 split. In the training cohort, univariate analysis of clinical information was performed to identify prognostic factors related to liver metastasis in panNET patients. Then, through multivariate analysis, independent prognostic factors related to liver metastasis were selected and applied to the nomogram model.

Model discrimination and accuracy were assessed based on the Harrell's concordance index (C-index), receiver operating characteristic (ROC) curve, and area

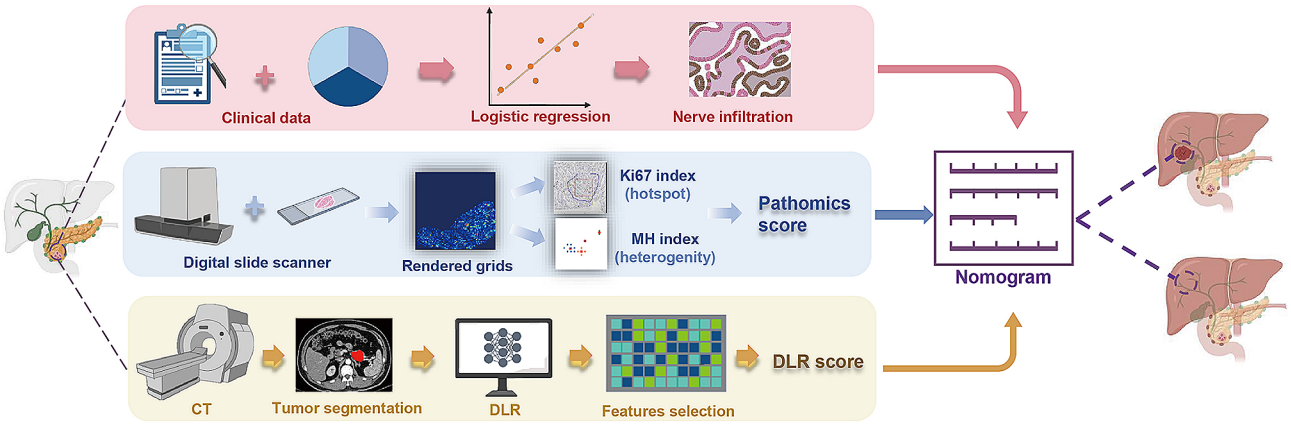

Fig. 2 Schematic illustration of the study design. Features were selected from clinical history, pathologic slides, and CT images. Logistic analysis of clinical information identified independent prognostic factors for liver metastasis. A computational pathology model was used to calculate the Ki67 index in hotspot areas and the MH index in heterogeneous distributions to determine the Pathomics score. The radiomics and deep learning models were used to analyze CT images to derive the DLR model. Finally, based on the total scores from the nomogram, patients were categorized into high- and low-risk groups for predicting postoperative liver metastasis

under the curve (AUC). The calibration curve was used to evaluate the alignment between the predicted and actual models. The Hosmer–Lemeshow goodness of fit test (HL test) was used to evaluate the degree of consistency between the observed and predicted outcomes. The clinical utility of the nomogram was evaluated using decision curve analysis (DCA) [13]. Additionally, we performed internal validation through a bootstrap resampling process to provide an unbiased estimate of model performance, with the C-index serving as the primary metric for evaluation.

Risk group stratification and statistical analysis

Based on the established nomogram model, the total predicted score for each patient was obtained by summing the scores corresponding to each relevant factor. To further distinguish patients at risk of liver metastasis, all patients were categorized into high- and low-risk groups based on the total scores from the nomogram. RFS was then compared between the groups.

Random grouping was performed using the R function "createDataPartition". Statistical analysis and nomogram analysis were conducted using SPSS version 25.0 software (IBM, Armonk, NY, USA) and R software version 4.3.1 (http://www.r-project.org). Continuous variables were compared using either Student's t-test or the Mann–Whitney U test, while categorical variables were assessed using the $\chi 2$ test or Yates' correction. The Delong test was used to employed to compare the diagnostic performance of various prediction models. Risk stratification was conducted based on the median total predicted score. Kaplan-Meier survival analysis was utilized, and the log-rank test was used to compare outcomes among different risk groups. Statistical significance in all analyses was defined as a two-tailed p value or adjusted p value less than 0.05. Variables with a p value less than 0.05 in the univariate logistic regression were chosen for inclusion in the multivariate logistic regression analysis. The calibration curve was determined using the bootstrapping method (1,000 intervals).

Results

Patient characteristics

This study included 163 panNET patients with available preoperative enhanced CT images and postoperative pathological slides (Table 1). Among these patients, 37 had postoperative liver metastasis, with an average tumor size of 4.79 cm. Of those with liver metastasis, 24 patients (64.9%) had vascular invasion, and 18 patients (48.6%) had nerve infiltration. The distribution of tumor grades in the liver metastasis group was as follows: 4 patients (10.8%) had G1 tumors, 30 patients (81.1%) had G2 tumors, and 3 patients (8.1%) had G3 tumors. In terms of tumor stage, there were 2 patients (5.4%) with T1 tumors, 23 patients (62.2%) with T2 tumors, and 12 patients (32.4%) with T3 tumors. The group without liver metastasis consisted of 126 panNET patients with an average tumor size of 2.69 cm. Among them, 65 patients (51.6%), 58 patients (46.0%), and 3 patients (2.4%) were classified as having G1, G2, and G3 tumors respectively, while 55 patients (43.7%), 60 patients (47.6%), and 11 patients (8.7%) had T1, T2, and T3 tumors, respectively.

The measurement of pathologic signatures

The Ki67 index was significantly greater in the group with liver metastasis (median: 0.10, IQR: 0.04–0.15) than in the group without liver metastasis (median: 0.02, IQR: 0.02–0.05) ($p<0.05$, Fig. 3A, B). Similarly, the MH index was significantly greater in the liver metastasis group (median: 0.18, IQR: 0.12–0.37) than in the group without

Table 1 The clinicopathological features of panNET patients in postoperative liver metastasis and non-liver metastasis groups

	Postoperative Liver Metastasis (*N* = 37)	Postoperative Non-Liver Metastasis (*N* = 126)	*P* value
Sex, *n* **(%)**			0.491
Male	20 (54.1%)	60 (47.6%)	
Female	17 (45.9%)	66 (52.4%)	
Age(y), median[range]			0.298
Mean (SD)	50.6 (10.5)	52.8 (11.7)	
Median [Min, Max]	52.0 [28.0, 71.0]	53.0 [25.0, 76.0]	
Tumor site, *n* **(%)**			0.782
Head/Neck	11 (29.7%)	40 (31.7%)	
Body/Tail	14 (37.8%)	40 (31.7%)	
Multiple locations	12 (32.4%)	46 (36.5%)	
Vascular invasion, *n* **(%)**			<0.001
Present	24 (64.9%)	18 (14.3%)	
Absent	13 (35.1%)	108 (85.7%)	
Nerve infiltration, *n* **(%)**			<0.001
Present	18 (48.6%)	18 (14.3%)	
Absent	19 (51.4%)	108 (85.7%)	
Grade, *n* **(%)**			<0.001
G1	4 (10.8%)	65 (51.6%)	
G2	30 (81.1%)	58 (46.0%)	
G3	3 (8.1%)	3 (2.4%)	
T stage, *n* **(%)**			<0.001
T1	2 (5.4%)	55 (43.7%)	
T2	23 (62.2%)	60 (47.6%)	
T3	12 (32.4%)	11 (8.7%)	
Lymph Node Metastasis, *n* **(%)**			<0.001
Present	17 (45.9%)	17 (13.5%)	
Absent	20 (54.1%)	109 (86.5%)	
Synchronous Liver Metastasis, *n* **(%)**			<0.001
Present	35 (94.6%)	4 (3.2%)	
Absent	2 (5.4%)	122 (96.8%)	
ATRX & DAXX, *n* **(%)**			0.967
Both positive	21 (56.8%)	72 (57.1%)	
Any negative	16 (43.2%)	54 (42.9%)	

liver metastasis (median: 0.07, IQR: 0.02–0.17) ($p<0.05$, Fig. 3C, D). The Pathomics score, which was derived from the combination of these two parameters, also exhibited statistically significant differences between the groups ($p<0.05$), with median values of 0.27 (IQR, 0.17–0.53) for the liver metastasis group and 0.15 (IQR, 0.12–0.18) for the group without liver metastasis.

The Ki67 index had an AUC of 0.794 (95% CI: 0.714–0.874) for predicting liver metastasis in panNET patients, while the MH index achieved a similar AUC of 0.753 (95% CI: 0.675–0.831). However, the prediction accuracy of the Pathomics score was even higher, with an AUC of 0.799 (95% CI: 0.724–0.874) for liver metastases (Fig. 3E).

The performance of radiomics and deep learning

A total of 2048 DL features and 1834 radiomics features were extracted. Following the ICC analysis, 1460 DL and 1344 radiomics features were retained (ICC>0.8). After examining the correlations and conducting the U test, 109 radiomics features and 278 deep learning features were selected for LASSO regression analysis. Subsequently, 8 DL and 10 radiomics features were utilized for model construction (Fig. 4A, B; Additional file 1: Figure S1). Each feature exhibited a correlation coefficient of less than 0.5 and a significance level of $p<0.05$ (Fig. 4C, D). In the radiomics training cohort, the AUC was 0.821 (95% CI: 0.671–0.971), and it was 0.807 (95% CI: 0.647–0.967) for the test cohort. The AUCs of the training and test cohorts for the DL model were 0.86 (95% CI: 0.741–0.978) and 0.795 (95% CI: 0.572-1), respectively. There were no significant differences between the training and test cohorts (Additional file 1: Figure S2).

Finally, the DLR score was developed by logistic regression with the radiomics score and DL score. The AUC of the radiomics model was 0.824 (95% CI: 0.720–0.927), and the AUC of the DL model was 0.844 (95%

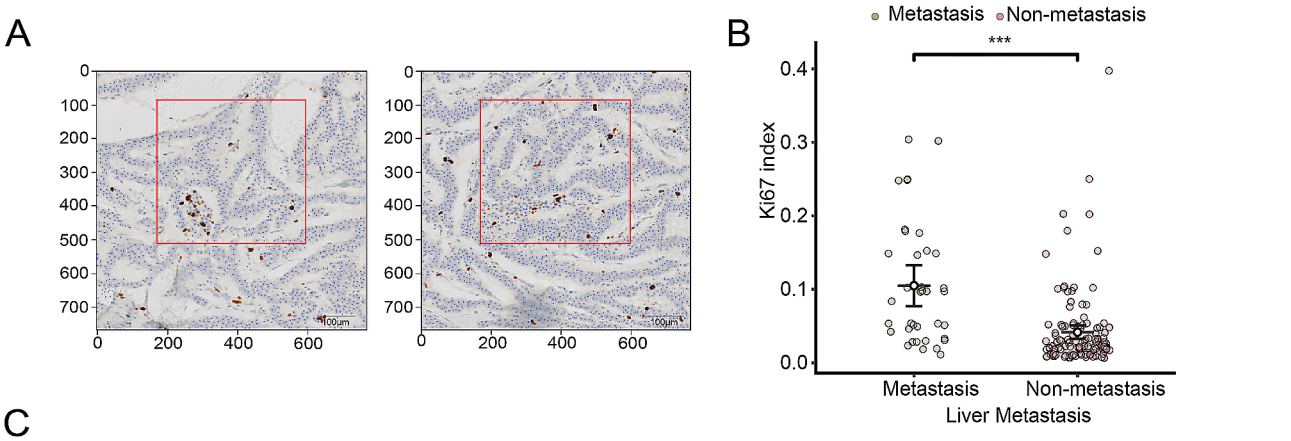

$$MH = \frac{2\,\sigma_i\, p_i^{neg} p_i^{pos}}{\sigma_i \left(p_i^{neg}\right)^2 + \sigma_i \left(p_i^{pos}\right)^2}$$

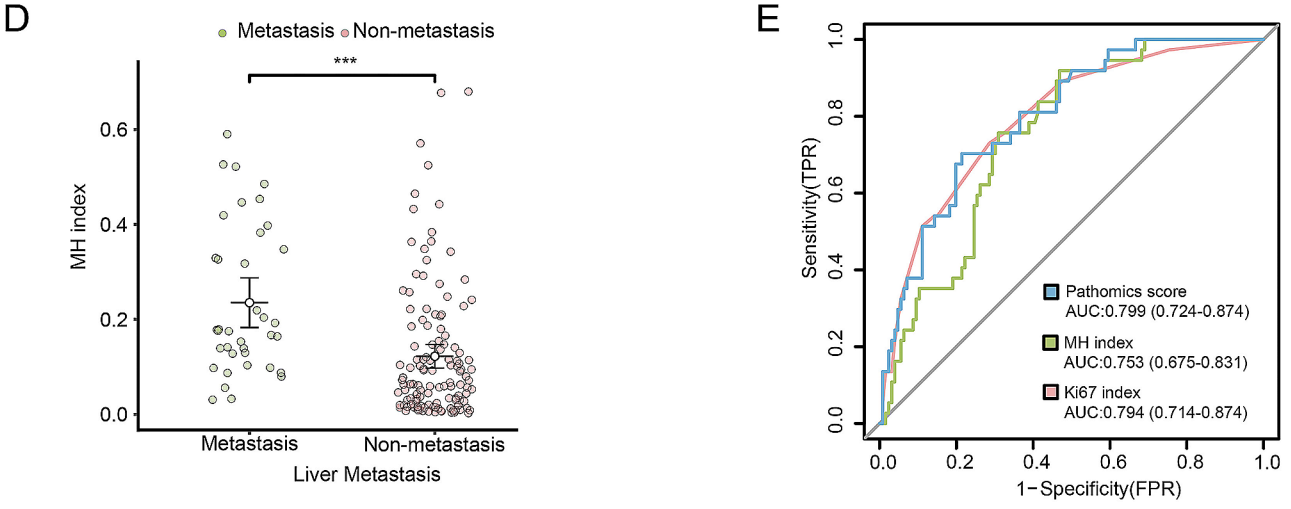

Fig. 3 The DIA of pathologic signatures. **A** Ki67 staining within WSIs was automatically analyzed in sliding windows. **B** The Ki67 index determined by the DIA was significantly greater in the group with liver metastasis than in the group without liver metastasis. **C** The DIA for Ki67 staining was used to calculate the distributions of Ki67-positive cells among the patients. One patient showed significant heterogeneity, while another had a more uniform distribution. The formula for calculating the heterogeneity index is provided below. **D** The heterogeneous distribution of the MH index was significantly greater in the liver metastasis group than in the group without liver metastasis. **E** The ROC curve indicated that the Pathomics score had better predictive ability than both the Ki67 index and MH index. n.s., $P > 0.05$; *$P \le 0.05$, **$P \le 0.01$, ***$P \le 0.001$ and ****$P \le 0.0001$

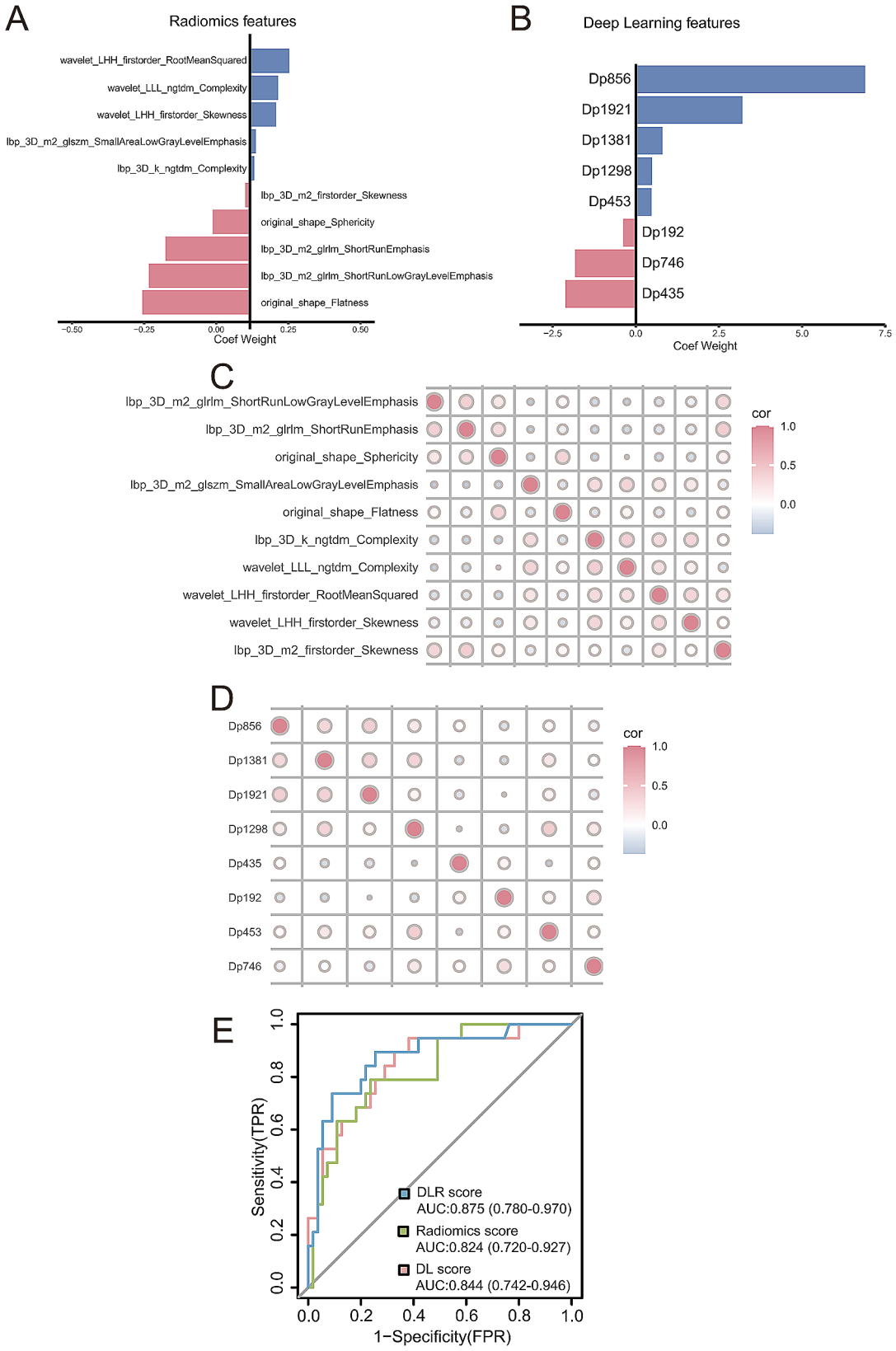

Fig. 4 Radiomics and deep learning analysis. **A** The coefficient weights of radiomics features. **B** The coefficient weights of the deep learning features. **C** The correlation dotplot of radiomics features. **D** The correlation dotplot of the deep learning features. **E** The ROC curve indicated that the DLR score has better predictive ability than radiomic features and deep learning

CI: 0.742–0.946). In contrast, the DLR model exhibited superior predictive ability, with an AUC=0.875 (95% CI: 0.780–0.970) (Fig. 4E). The Delong test showed no significant differences between the DLR model and the Pathomics model (p=0.903).

Integrated nomogram for predicting liver metastasis

Univariate logistic analysis of clinical information in the training group revealed a significant relationship between vascular invasion (p=0.007), nerve infiltration (p=0.001) and T stage (p=0.038 and p=0.013) with liver metastasis (Table 2). Further multivariate analysis revealed that only nerve infiltration was an independent prognostic factor for liver metastasis in panNET patients (p=0.007). This independent clinical factor, along with the Pathomics score and DLR score, were used to construct an integrated nomogram. Additionally, the attention map of Ki67 distribution and radiomics/deep learning features served as an interpretable visualization tool for model prediction (Fig. 5). To determine the probability of liver metastasis in panNET patients, each risk factor was assigned a score based on its corresponding value. These scores were then added together to obtain the total points. The probability of liver metastasis can be represented by drawing a line downward from the total points line (Fig. 6A).

In the performance test, the nomogram model achieved an AUC of 0.985 (95% CI: 0.960-1.000) in the training cohort and 0.961 (95% CI: 0.896-1.000) in the validation cohort (Fig. 6B, C). The contributions to the predictive model were as follows: a Pathomics score of 58%, a DLR score of 32%, and a clinical factor of nerve infiltration of 10% (Fig. 6D). The HL test results for both cohorts showed no statistically significant differences (p=0.999, p=0.588), indicating a close alignment between the predicted and actual values. The calibration curve further confirmed this strong performance by showing no significant differences between the predicted and actual models (Additional file 1: Figure S3). The internal validation results, with a C-index of 0.969 (95% CI: 0.968, 0.999), demonstrated that employing bootstrap resampling yielded a robust and unbiased estimate of the model's performance. Additionally, the DCA curve demonstrated that the nomogram model exhibited greater net benefit than the other single-factor models across a wide range of threshold probabilities in both the training and validation cohorts (Fig. 6E, F). These findings suggest that the combined model is more clinically advantageous.

A novel model for predicting patient survival

A total of 163 patients were included in our follow-up study. Among them, 35 patients experienced recurrence,

Table 2 Univariate and multivariate logistics analyses on variables for the prediction of liver metastasis of the panNET patients in the training cohort

Characteristics	Univariate analysis		Multivariate analysis	
	Odds Ratio (95% CI)	*P* value	Odds Ratio (95% CI)	*P* value
Sex				
Male	1.000(Reference)			
Female	0.464(0.121–1.779)	0.263		
Age(years)	0.964 (0.908–1.024)	0.233		
Tumor site				
Head/Neck	1.000(Reference)			
Body/Tail	1.875 (0.336–10.463)	0.474		
Multiple locations	0.750 (0.136–4.127)	0.741		
Vascular Invasion				
Present	1.000(Reference)		1.000(Reference)	
Absent	0.128 (0.029–0.566)	**0.007**	0.983 (0.073–13.211)	0.989
Nerve Infiltration				
Present	1.000(Reference)		1.000(Reference)	
Absent	46.500 (6.702–322.612)	**0.001**	40.792 (2.770–600.685)	**0.007**
T stage				
T1	1.000(Reference)		1.000(Reference)	
T2	10.500(1.142–96.576)	**0.038**	1.467(0.075–28.713)	0.800
T3	24.000(1.952–295.061)	**0.013**	7.405(0.424–129.269)	0.170
Lymph Node Metastasis				
Present	1.000(Reference)			
Absent	0.200(0.037–1.082)	0.062		
ATRX & DAXX				
Both positive	1.000(Reference)			
Any negative	0.600(0.151–2.390)	0.469		

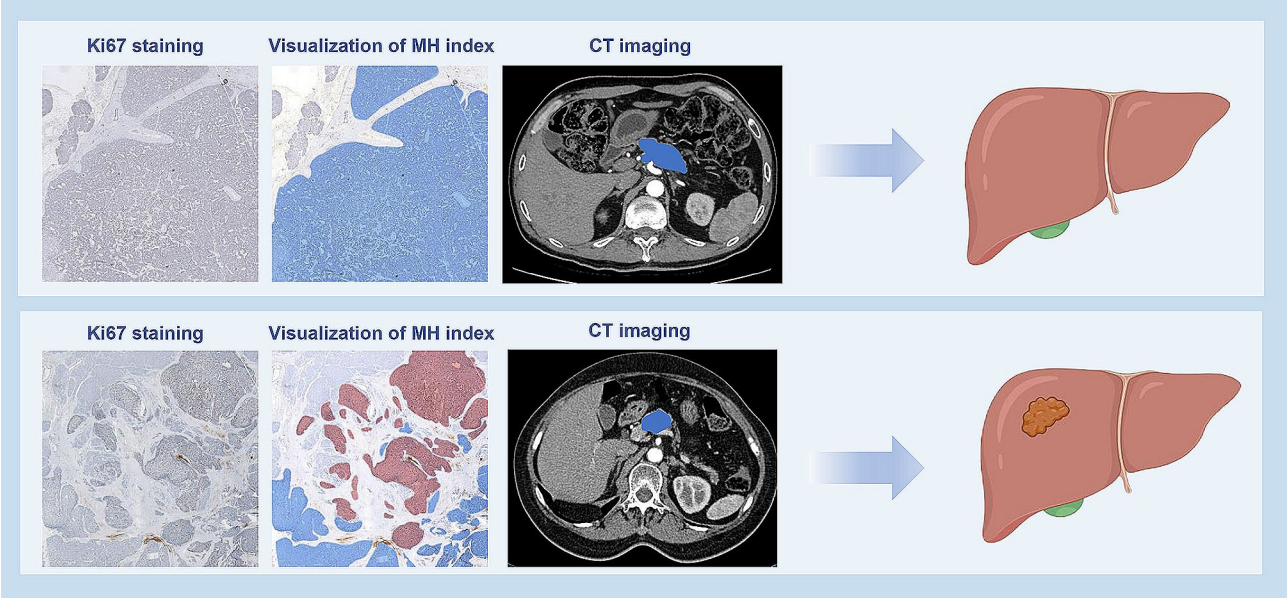

Fig. 5 Visualization of the nomogram for predicting postoperative liver metastasis. As shown above, one patient exhibited low heterogeneity in Ki67 staining under DIA analysis, along with a low imaging DLR score, indicating that this patient is a low-risk group for postoperative liver metastasis. As shown below, another patient displayed high heterogeneity in Ki67 staining with uneven distribution in the DIA. When combined with DLR score analysis, this patient was classified as a high-risk group for postoperative liver metastasis

with 2 patients developing liver metastasis during the observation period. Three patients who died without experiencing recurrence and were censored at the date of death. The median RFS was 31.78 months, ranging from 0.8 to 62.7 months.

According to our predictive model, all patients were divided into two risk levels. The cut-off value, represented by the median total predicted score, was 25.1. The median RFS for the high-risk group was 28.5 months, while for the low-risk group, it was 34.7 months ($p < 0.0001$, Fig. 6G).

Discussion

Based on the digital analysis of pathological and radiological images, we developed a specific and integrated model for predicting liver metastasis in postoperative panNET patients. Liver metastasis is an important prognostic factor for patients with panNET, with metachronous metastases identified in approximately 50% of patients during postoperative follow-up [14]. Previous studies that examined clinical medical history and pathological reports have revealed a correlation between liver metastasis and certain clinical pathological features, such as tumor size and histological grade [15, 16]. These sources of information contain valuable data related to disease outcomes that may improve prediction accuracy. In this study, we calculated the hotspot index and Ki67 heterogeneity distribution to create a Pathomics score, which offers a detailed microscopic assessment of panNETs. Then, by combining overall radiomics and deep learning, we developed a new network to accurately predict postoperative liver metastasis in panNET patients.

The Ki67 index determined via immunohistochemistry is a widely accepted prognostic marker for panNETs [17]. It can also be used to predict the risk of recurrence and metastasis in panNET patients who have undergone surgical resection [18]. Various methods are available for Ki67 scoring, including manual counting by pathologists, automated microscopy and software counting, and reverse transcription-quantitative polymerase chain reaction [19]. Manual Ki67 counting based on immunohistochemically stained sections remains the most commonly used method in clinical practice. Currently, there is a growing interest in using DIA to assess the Ki67 index. A comparative meta-analysis showed that DIA and manual counting have a high level of agreement (coefficient of concordance: 0.94, 95% CI: 0.83–0.98) [20]. DIA provides more objective and consistent results, with accuracy comparable to that of manual counting but with greater efficiency. Specifically, Ki-67 staining obtained from panNET patients is well suited for DIA because of the uniform cellular morphology of NETs, which allows the model to recognize tumor cells and analyze their distribution. Furthermore, both a single-cell RNA sequencing study and our previous findings indicate that spatiotemporal heterogeneity and the spatial distribution of Ki67-positive cells are associated with malignant progression and patient prognosis, respectively, in panNET patients [9, 21]. Additionally, the ecological MH index can be used to calculate and compare the heterogeneity

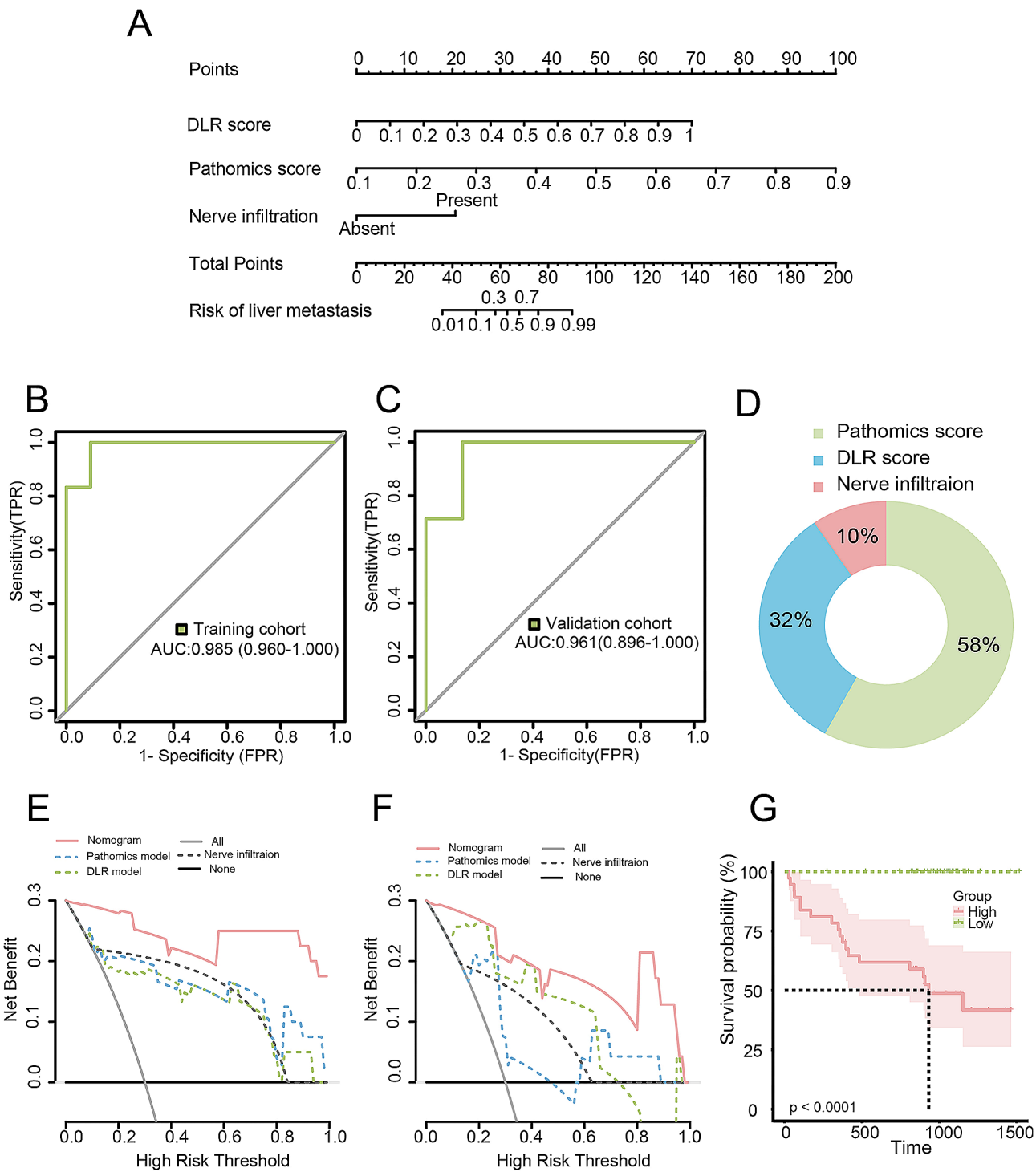

Fig. 6 Comprehensive evaluation of the combination model. **A** Combined nomogram for predicting the risk of liver metastasis. **B-C** Both the training and validation cohorts exhibited notable predictive power of the model, as illustrated by the ROC curve. **D** Contribution to the predictive model of each factor. **E-F** The calibration curves for the nomogram show that the combined model yields greater net benefits at nearly all threshold probabilities in both the training and validation sets. **G** Kaplan–Meier plots for recurrence–free survival (RFS) curves demonstrating significant differences between the low- and high-risk groups

of tumor proliferation in NETs. Therefore, to comprehensively assess the pathological characteristics of the primary pancreatic lesion, we measured both the hotspot index and heterogeneity MH index via Ki67 staining. Our findings indicate that both the Ki67 index and MH index were significantly greater in the liver metastasis group, with AUCs of 0.794 and 0.753, respectively, for predicting liver metastasis. When combined with the Pathomics score, superior prediction accuracy was achieved, with an AUC of 0.799 for patients with liver metastases.

The rapid development of imaging technology, including PET/CT and PET/MRI, has not sufficiently improved the detection sensitivity for low-proliferative NET metastases [22]. Somatostatin receptor-labeled nuclear medicine imaging holds promise in this regard, but its clinical application is limited due to the need for specialized instruments [23, 24].Despite this, CT scans remain commonly used for routine liver metastasis screening [25]. However, due to the low specificity of CT for detecting microscopic lesions, recent studies have explored the use of radiomics or deep learning for predicting the outcomes of panNET patients [26, 27]. Homps et al. developed a radiomics model using preoperative CT data that predicts recurrence-free survival in patients with panNET [28]. Moreover, Yang et al. evaluated a deep learning radiomics model that greatly improved the ability to predict overall survival in patients with gastric neuroendocrine neoplasms [29]. Similarly, our previous study revealed that the DLR signature of the primary lesion is more closely associated with panNET metastasis than radiomics [12]. Likewise, in this study, we observed that the radiomics model had an AUC of 0.824 in predicting liver metastasis in panNET patients, while the DL model had a separate AUC value of 0.844. By combining the DL and radiomics scores with the DLR, an increase in the AUC was achieved (0.875), suggesting that this synergistic approach to radiological image analysis offers optimal predictive power for liver metastasis in panNET patients who have undergone resection.

Integrating different perspectives, including clinical, pathological, and radiological features, can improve the understanding and prediction of tumors. Wang et al. [30]. reported a combined nomogram using pathomics and radiomics, which showed improved accuracy in predicting patient survival compared to using pathomics or radiomics alone for colorectal cancer lung metastasis. However, for rare neuroendocrine tumors, there are limited predictive models based on clinical pathological textual data or radiological imaging. Pan et al. [16]. previously developed a nomogram for predicting liver metastasis with C-indexes of 0.850 and 0.846 for the training and validation cohorts, respectively. Pulvirenti et al. [31]. created a nomogram for estimating survival in panNET patients postresection, with a C-index of 0.84 in a multi-institutional cohort. Utilizing radiomics technology, An et al. [32] developed a CT radiomics model for predicting gastrointestinal pancreatic neuroendocrine neoplasm recurrence with an AUC of 0.712, which improved to 0.824 when integrated with clinical data. In this study, novel Ki67 heterogeneity and radiological DLR scores were first incorporated into a predictive model to enhance its performance. This integrated model provides accurate predictions for postoperative liver metastasis in panNET patients (AUC=0.978), surpassing both individual data models and previous models. The stratified results based on the model-assigned risk factors indicated a significant difference in patient RFS ($p<0.0001$). These findings confirmed that evaluating the prognosis accurately is enhanced by taking into account various clinicopathological and radiological perspectives. By expanding on this pathology-imaging model, incorporating additional medical information in a multimodal analysis can yield more precise predictions.

It is crucial to recognize the constraints inherent in our predictive model. First, the number of patients included in this study was limited, as long-term follow-up is needed to confirm cases of postoperative liver metastasis in panNET patients. Second, this study included two types of patients with R0 resected panNET: those who underwent resection of the pancreatic primary lesion only and those who underwent combined resection of the primary lesion and simultaneous liver metastases. Despite having different tumor stages, both groups required postoperative treatment guidance and prediction of metastasis, so both groups were included in this study. Third, we relied on internal validation for model assessment due to data limitations. To minimize bias, we employed a bootstrap resampling method with 1000 iterations, as suggested by a previous study [33]. In the future, a multicenter and large cohort study should be conducted to validate our model.

Conclusion

In conclusion, we developed an integrated model that combines a computational pathologic index and deep learning-radiomics. This model provides a more precise prediction of liver metastases in postoperative panNETs than do individual data models and can assist clinicians in making personalized treatment decisions following R0 resection surgery in panNET patients.

Supplementary Information

The online version contains supplementary material available at https://doi.org/10.1186/s12967-024-05449-4.

Supplementary Material 1

Supplementary Material 2

Acknowledgements
Not applicable.

Author contributions
Mengke Ma and Wenchao Gu: Data curation, Writing- Original draft preparation, Conceptualization, Methodology. Yun Liang and Xueping Han: Visualization, Investigation, Resources. Meng Zhang and Midie Xu: Software, Validation. Dan Huang, Wei Tang and Heli Gao: Investigation, Resources, Writing- Reviewing and Editing.

Funding
This work was supported by the Shanghai Engineering Research Center of Artificial Intelligence Technology for Neoplastic Diseases (Grant No. 19DZ2251800, Huang), the Clinical Research Special Project of Shanghai Municipal Health Commission (Grant No.202340123, Tang), and the JSPS KAKENHI (Grant No. JP22K20814, Gu).

Data availability
The datasets used and/or analyzed during the current study are available from the corresponding author on reasonable request.

Declarations

Ethics approval and consent to participate
This study was conducted in accordance with the Declaration of Helsinki and approved by the Ethical Committee for Clinical Research at Fudan University Shanghai Cancer Center (No. 050432-4-2108).

Competing interests
The authors declare no competing interests.

Author details
[1]Department of Pathology, Fudan University Shanghai Cancer Center, Shanghai, China
[2]Department of Oncology, Fudan University Shanghai Medical College, Shanghai, China
[3]Institute of Pathology, Fudan University, Shanghai, China
[4]Department of Diagnostic and Interventional Radiology, Faculty of Medicine, University of Tsukuba, Ibaraki, Tsukuba, Japan
[5]Department of Radiology, Fudan University Shanghai Cancer Center, Shanghai, China
[6]Department of Diagnostic Radiology and Nuclear Medicine, Gunma University Graduate School of Medicine, Maebashi, Japan
[7]Centre for Neuroendocrine Tumors, Fudan University Shanghai Cancer Center, Shanghai, China
[8]Department of Pancreatic Surgery, Fudan University Shanghai Cancer Center, Shanghai, China

Received: 10 April 2024 / Accepted: 27 June 2024
Published online: 14 August 2024

References

1. Sonbol MB, Mazza GL, Mi L, Oliver T, Starr J, Gudmundsdottir H, et al. Survival and incidence patterns of pancreatic neuroendocrine tumors over the last 2 decades: a SEER database analysis. Oncologist. 2022;27:573–8. https://doi.org/10.1093/oncolo/oyac049.
2. Ito T, Igarashi H, Nakamura K, Sasano H, Okusaka T, Takano K, et al. Epidemiological trends of pancreatic and gastrointestinal neuroendocrine tumors in Japan: a nationwide survey analysis. J Gastroenterol. 2015;50:58–64. https://doi.org/10.1007/s00535-014-0934-2.
3. Kaslow SR, Hani L, Cohen SM, Wolfgang CL, Sacks GD, Berman RS, et al. Outcomes after primary tumor resection of metastatic pancreatic neuroendocrine tumors: an analysis of the National Cancer Database. J Surg Oncol. 2023;128:262–70. https://doi.org/10.1002/jso.27280.
4. Frilling A, Modlin IM, Kidd M, Russell C, Breitenstein S, Salem R et al. Recommendations for management of patients with neuroendocrine liver metastases. Lancet Oncol 15: e8-e21, 2014.https://doi.org/10.1016/S1470-2045(13)70362-0.
5. Chu QD, Hill HC, Douglass HO Jr., Driscoll D, Smith JL, Nava HR, et al. Predictive factors associated with long-term survival in patients with neuroendocrine tumors of the pancreas. Ann Surg Oncol. 2002;9:855–62. https://doi.org/10.1007/BF02557521.
6. Jilesen AP, van Eijck CH, in't Hof KH, van Dieren S, Gouma DJ, van Dijkum EJ. Postoperative complications, In-Hospital mortality and 5-Year Survival after Surgical Resection for patients with a pancreatic neuroendocrine tumor: a systematic review. World J Surg. 2016;40:729–48. https://doi.org/10.1007/s00268-015-3328-6.
7. Chen J, Yang Y, Liu Y, Kan H. Prognosis analysis of patients with pancreatic neuroendocrine tumors after surgical resection and the application of enucleation. World J Surg Oncol. 2021;19:11. https://doi.org/10.1186/s12957-020-02115-z.
8. Canellas R, Burk KS, Parakh A, Sahani DV. Prediction of pancreatic neuroendocrine tumor Grade based on CT Features and texture analysis. AJR Am J Roentgenol. 2018;210:341–6. https://doi.org/10.2214/ajr.17.18417.
9. Zhang M, Tan C, Wang X, Ding X, Zhang B, Yang Z, et al. Digital Image Analysis of Ki67 heterogeneity improves the diagnosis and prognosis of gastroenteropancreatic neuroendocrine neoplasms. Mod Pathol. 2023;36:100017. https://doi.org/10.1016/j.modpat.2022.100017.
10. La Diagnostic RS. Prognostic, and predictive role of Ki67 proliferative index in neuroendocrine and endocrine neoplasms: past, Present, and Future. Endocr Pathol. 2023;34:79–97. https://doi.org/10.1007/s12022-023-09755-3.
11. Gu D, Hu Y, Ding H, Wei J, Chen K, Liu H, et al. CT radiomics may predict the grade of pancreatic neuroendocrine tumors: a multicenter study. Eur Radiol. 2019;29:6880–90. https://doi.org/10.1007/s00330-019-06176-x.
12. Gu W, Chen Y, Zhu H, Chen H, Yang Z, Mo S, et al. Development and validation of CT-based radiomics deep learning signatures to predict lymph node metastasis in non-functional pancreatic neuroendocrine tumors: a multicohort study. EClinicalMedicine. 2023;65:102269. https://doi.org/10.1016/j.eclinm.2023.102269.
13. Fitzgerald M, Saville BR, Lewis RJ. Decision curve analysis. JAMA. 2015;313:409–10. https://doi.org/10.1001/jama.2015.37.
14. Centonze DC, Cinardi N, Giannone G. Surgical resection for neuroendocrine tumors of the pancreas: a fourteen years single institutional observation. Eur Rev Med Pharmacol Sci. 2014;18:32–5.
15. Li J, Huang L, Liao C, Liu G, Tian Y, Chen S. Two machine learning-based nomogram to predict risk and prognostic factors for liver metastasis from pancreatic neuroendocrine tumors: a multicenter study. BMC Cancer. 2023;23:529. https://doi.org/10.1186/s12885-023-10893-4.
16. Pan M, Yang Y, Teng T, Lu F, Chen Y, Huang H. Development and validation of a simple-to-use nomogram to predict liver metastasis in patients with pancreatic neuroendocrine neoplasms: a large cohort study. BMC Gastroenterol 21: 1012021.https://doi.org/10.1186/s12876-021-01685-w.
17. Lopez-Aguiar AG, Ethun CG, Postlewait LM, Zhelnin K, Krasinskas A, El-Rayes BF, et al. Redefining the Ki-67 Index Stratification for Low-Grade pancreatic neuroendocrine tumors: improving its prognostic value for recurrence of Disease. Ann Surg Oncol. 2018;25:290–8. https://doi.org/10.1245/s10434-017-6140-8.
18. Genç CG, Falconi M, Partelli S, Muffatti F, van Eeden S, Doglioni C, et al. Recurrence of pancreatic neuroendocrine tumors and Survival predicted by Ki67. Ann Surg Oncol. 2018;25:2467–74. https://doi.org/10.1245/s10434-018-6518-2.
19. Li LT, Jiang G, Chen Q, Zheng JN. Ki67 is a promising molecular target in the diagnosis of cancer (review). Mol Med Rep. 2015;11:1566–72. https://doi.org/10.3892/mmr.2014.2914.
20. Luchini C, Pantanowitz L, Adsay V, Asa SL, Antonini P, Girolami I, et al. Ki-67 assessment of pancreatic neuroendocrine neoplasms: systematic review and meta-analysis of manual vs. digital pathology scoring. Mod Pathol. 2022;35:712–20. https://doi.org/10.1038/s41379-022-01055-1.
21. Zhou Y, Liu S, Liu C, Yang J, Lin Q, Zheng S, et al. Single-cell RNA sequencing reveals spatiotemporal heterogeneity and malignant progression in pancreatic neuroendocrine tumor. Int J Biol Sci. 2021;17:3760–75. https://doi.org/10.7150/ijbs.61717.
22. Sundin A, Arnold R, Baudin E, Cwikla JB, Eriksson B, Fanti S, et al. ENETS Consensus guidelines for the standards of Care in Neuroendocrine tumors: Radiological, Nuclear Medicine and Hybrid Imaging. Neuroendocrinology. 2017;105:212–44. https://doi.org/10.1159/000471879.
23. Gabriel M, Decristoforo C, Kendler D, Dobrozemsky G, Heute D, Uprimny C, et al. 68Ga-DOTA-Tyr3-octreotide PET in neuroendocrine tumors: comparison with somatostatin receptor scintigraphy and CT. J Nucl Med. 2007;48:508–18. https://doi.org/10.2967/jnumed.106.035667.

24. Frilling A, Sotiropoulos GC, Radtke A, Malago M, Bockisch A, Kuehl H, et al. The impact of 68Ga-DOTATOC positron emission tomography/computed tomography on the multimodal management of patients with neuroendocrine tumors. Ann Surg. 2010;252:850–6. https://doi.org/10.1097/SLA.0b013e3181fd37e8.
25. Rockall AG, Reznek RH. Imaging of neuroendocrine tumours (CT/MR/US). Best Pract Res Clin Endocrinol Metab. 2007;21:43–68. https://doi.org/10.1016/j.beem.2007.01.003.
26. Huang B, Lin X, Shen J, Chen X, Chen J, Li ZP, et al. Accurate and feasible deep learning based semi-automatic segmentation in CT for Radiomics Analysis in pancreatic neuroendocrine neoplasms. IEEE J Biomed Health Inf. 2021;25:3498–506. https://doi.org/10.1109/jbhi.2021.3070708.
27. Mori M, Palumbo D, Muffatti F, Partelli S, Mushtaq J, Andreasi V, et al. Prediction of the characteristics of aggressiveness of pancreatic neuroendocrine neoplasms (PanNENs) based on CT radiomic features. Eur Radiol. 2023;33:4412–21. https://doi.org/10.1007/s00330-022-09351-9.
28. Homps M, Soyer P, Coriat R, Dermine S, Pellat A, Fuks D, et al. A preoperative computed tomography radiomics model to predict disease-free survival in patients with pancreatic neuroendocrine tumors. Eur J Endocrinol. 2023;189:476–84. https://doi.org/10.1093/ejendo/lvad130.
29. Yang Z, Han Y, Li F, Zhang A, Cheng M, Gao J. Deep learning radiomics analysis based on computed tomography for survival prediction in gastric neuroendocrine neoplasm: a multicenter study. Quant Imaging Med Surg. 2023;13:8190–203. https://doi.org/10.21037/qims-23-577.
30. Wang R, Dai W, Gong J, Huang M, Hu T, Li H, et al., et al. Development of a novel combined nomogram model integrating deep learning-pathomics, radiomics and immunoscore to predict postoperative outcome of colorectal cancer lung metastasis patients. J Hematol Oncol. 2022;15(11). https://doi.org/10.1186/s13045-022-01225-3.
31. Pulvirenti A, Javed AA, Landoni L, Jamieson NB, Chou JF, Miotto M, et al. Multi-institutional development and external validation of a Nomogram to predict recurrence after curative resection of pancreatic neuroendocrine tumors. Ann Surg. 2021;274:1051–7. https://doi.org/10.1097/sla.0000000000003579.
32. An P, Zhang J, Li M, Duan P, He Z, Wang Z, et al. Clinical Data-CT Radiomics-based model for Predicting prognosis of patients with gastrointestinal pancreatic neuroendocrine neoplasms (GP-NENs). Comput Math Methods Med. 2022;41863052022. https://doi.org/10.1155/2022/4186305.
33. Johnson RW. An introduction to the bootstrap. Teach Stat. 2001;23:49–54. https://doi.org/10.1111/1467-9639.00050.

Publisher's Note